Two-dimensional electric-field vector measurement by a $LiTaO_3$ electro-optic probe tip

Wen-Kai Kuo, Wei-Hsuan Chen, Yang-Tung Huang, and Sheng-Lung Huang

An electro-optic probe tip that is made from LiTaO crystal to make tangentially two-dimensional electric-field (E-field) vector measurements is presented. We combine a new electro-optic modulation technique and a conventional one to resolve the two E-field components. The new modulation effect on the optical probing beam is caused by rotation of the principal axis the electro-optic crystal, which is proportional to the E-field. Inasmuch as there is no free charge involved in the axis rotation, rotation modulation of the axis can be as fast as conventional modulation. The principles are carefully derived, and an experimental system constructed, to measure two-dimensional E-field vectors on a test pattern. The results are in good agreement with those obtained with commercial software for electromagnetic simulation. The sensitivities of two tangential E-field components are 76 (mV/cm)/$\sqrt{\text{Hz}}$ and 0.8 (V/cm)/$\sqrt{\text{Hz}}$, respectively. The root-mean-square error of an E-field directional measurement is 1.5°.

OCIS codes: 120.5410, 230.2090, 230.4110, 130.6010.

1. Introduction

To meet testing requirements of modern microelectronics, optoelectronic techniques for probing semiconductor devices and circuits have been proposed with which the device or circuit parameters, such as response time, delay time, and scattering parameters, can be extracted.[1–4] Among these techniques, electro-optic (EO) probing–sensing has been the most powerful tool for characterizing electronic devices and circuits. With this technique, a two-dimensional field map of a GaAs circuit was obtained.[5] The EO probing technique can be categorized into two types, direct and external EO probing. Direct EO probing can be applied to a substrate that exhibits the EO effect,[6] whereas external EO probing can be applied to any substrate. For external EO sensing, a probe tip made from an EO material such as $LiTaO_3$ or GaAs is placed above the devices or circuits under test (DUT) so that the electric field (E-field) interacts with the probe laser beam by means of the EO material. One can use a pulsed laser to sample the signal on the DUT,[7] and a continuous-wave laser to obtain the real-time signal.[8,9] This approach benefits from its noncontact with and noninvasiveness of the DUT.

However, with these techniques, only the E-field strength can be measured. In addition to those of the field amplitudes, the values of the field orientations are also important for characterizing some microwave devices, such as chamfered bending transmission lines and patch antennae.[10] The EO probing technique can be used for this purpose. This technique was recently used for near-field mapping of a radiation pattern above a microwave resonator for E-field components along various axes.[11] It was also used to characterize the performance of planar antennae.[12,13] The publications cited above have reported the use of different kinds of EO material to measure the E-field components of different axes. Using different EO materials not only complicates the measurement but also decreases its accuracy because of the multiple calibrations involved. If values of the E-field components in more than one axis could be obtained with a single EO material, measurement and data analysis procedures could be greatly simplified.

Previously,[14,15] the E-field directions on a DUT were measured with laser beams with different propagation paths. This method requires some calcula-

W.-K. Kuo and Y.-T. Huang are with the Department of Electronics Engineering and Institute of Electronics, National Chiao Tung University, Taiwan, China. W.-K. Kuo (perry@pidc.gov.tw) is also with the Precision Instrument Development Center, 20 R&D Road VI, Hsinchu Science-Based Industrial Park, Hsinchu, Taiwan. W.-H. Chen and S.-L. Huang are with the Institute of Electro-Optical Engineering, National Sun Yat-Sen University, Taiwan.

Received 10 January 2000; revised manuscript received 12 June 2000.

0003-6935/00/274985-09$15.00/0

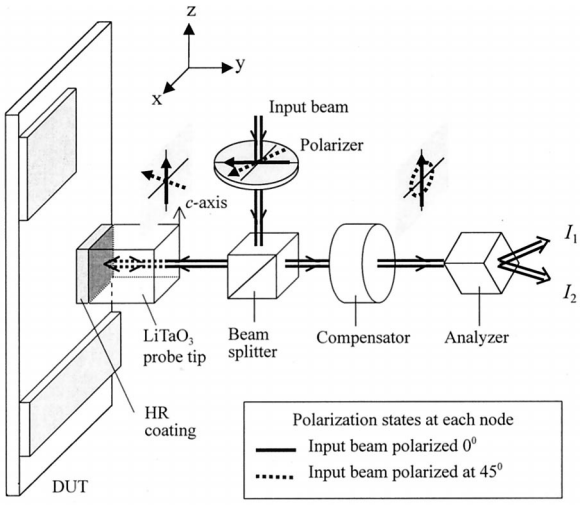

Fig. 1. External EO probing system with a HR probe tip.

tions to yield an E-field vector. Because this extra calculation step is needed, the method may be not suitable for a sampling system that uses a pulsed laser with a high repetition rate or for a real-time system that uses a continuous-wave laser to measure high-speed circuits. In this paper we present a novel two-dimensional (2-D) E-field vector measurement made with a $LiTaO_3$ EO probe tip with high sensitivity. We combine a new EO modulation technique with a conventional one to resolve two E-field components. For the conventional modulation technique, the modulation effect on the probing beam is due to compressed–stretched deformation of the index ellipsoid, whereas for the new modulation technique it results from rotation of the EO principal axis, which is proportional to the applied E field. Two components of an E-field vector can be obtained directly from two beams by different modulation techniques; therefore the techniques benefit from the elimination of the calculation step. The principle of the new modulation technique is discussed in detail below. Two kinds of probe tip are analyzed. An experimental system is constructed to verify the idea. The experimental results are compared with the simulation results obtained by a commercial Ansoft Maxwell three-dimensional field simulator.

2. Principle

An external EO probing system is shown in Fig. 1,[3] where the principal axes of the EO crystal are also indicated. A y-cut $LiTaO_3$ probe tip, one of the most widely used tips in EO probing systems, with a high-reflection (HR) coating on the bottom surface is used. For a $LiTaO_3$ crystal, the EO tensor is

$$[r_{ij}] = \begin{bmatrix} 0 & -r_{22} & r_{13} \\ 0 & r_{22} & r_{13} \\ 0 & 0 & r_{33} \\ 0 & r_{51} & 0 \\ r_{51} & 0 & 0 \\ -r_{22} & 0 & 0 \end{bmatrix}, \tag{1}$$

where $r_{13} = 8.4 \times 10^{-12}$ m/V, $r_{33} = 30.5 \times 10^{-12}$ m/V, $r_{22} = -0.2 \times 10^{-12}$ m/V, and $r_{51} = 22 \times 10^{-12}$ m/V for a 0.633-μm wavelength at low frequencies.[16] When a z-axis component (E_z) of an electric field is probed, its index ellipse equation that corresponds to the probe beam with a propagation direction along the y axis becomes

$$\left(\frac{1}{n_o^2} + r_{13}E_z\right)x^2 + \left(\frac{1}{n_e^2} + r_{33}E_z\right)z^2 = 1, \tag{2}$$

where $n_o = 2.176$ and $n_e = 2.180$. The principal axes of Eq. (2) will not rotate when E_z is applied, because E_z does not introduce any cross term into this equation. However, E_z can cause a change Δn in the index difference between two beams with polarizations along the two principal axes, the x and the z axes. Δn is the index difference caused by the EO effect only and does not include the static portion, which is $n_e - n_o$. If the probe beam is polarized at 45° with respect to the x axis, there are two equal polarization components along the x and z axes. The retardation between these two components caused by E_z is proportional to the intensity difference between two output beams.[3] Assuming that the crystal's voltage drop is much smaller than its half-wave voltage, the change in EO index difference is proportional to E_z and can be written as

$$\Delta n = k_{\Delta n}E_z, \tag{3}$$

where $k_{\Delta n} = 1.14 \times 10^{-10}$ m/V is the coefficient of the change of the EO-index difference. For simplicity, the E field is assumed to be uniformly applied to the crystal; the intensity difference between two output beams for this HR-type of probe tip can be expressed as

$$\Delta I_{\Delta n,\mathrm{HR}} = I_o \frac{2\pi}{\lambda} k_{\Delta n} 2LE_z, \tag{4}$$

where I_o is the summation of the time-averaged intensities of two output beams, $2L$ is the total interaction length between the E field and the optical beam in the crystal from the input to the output, and λ is the wavelength of the optical beam in vacuum. This is the conventional modulation technique used in an EO probing system. One can obtain E_z by measuring $\Delta I_{\Delta n,\mathrm{HR}}$, which is induced by the effect of the EO compressed–stretched deformation of the index ellipsoid. Meanwhile, for $LiTaO_3$ crystal, the coefficient of the change in the EO-index difference for the other tangential component E_x of the E field along the x axis is $\sim 6.3 \times 10^{-14}$ m/V. This value is negligible compared with that of E_z. Moreover, even if E_x induces a slight rotation of the principal axes, it can be shown that the effect of E_x is negligible in this configuration (see Appendix A).

To probe E_x we propose a the new modulation technique. For E_x measurement, the system configuration is the same as for measuring E_z, except that the input probe beam is polarized along the z axis, as

shown in Fig. 1. For this arrangement the intensity modulation in the probe beam is induced by the effect of rotation of the EO's principal axis instead of by compressed–stretched deformation of the index ellipsoid. The physical mechanism employed in the principal-axis rotation is still the linear EO effect; thus no free charges are involved in the modulation. Therefore this axis-rotation modulation can be as fast as the compressed–stretched deformation. Meanwhile, because the input beam is polarized along the z axis, the effect of the E_z component on the probe beam is phase delay only; thus the intensity difference for this configuration is insensitive to E_z.

For the same propagation direction along the y axis, the corresponding index ellipse equation with applied E_x is

$$\frac{x^2}{n_o^{\,2}} + \frac{z^2}{n_e^{\,2}} + 2r_{51}E_x xz = 1. \tag{5}$$

Because E_x introduces a cross term into the index ellipse equation and the coefficients of x^2 and z^2 are different, the new principal axes are slightly rotated, and this rotation angle $\Delta\theta$ can be approximated as

$$\Delta\theta \approx \frac{r_{51}E_x}{1/n_o^{\,2} - 1/n_e^{\,2}} = k_{\Delta\theta}E_x. \tag{6}$$

Substituting all these values into approximation (6) we obtain $k_{\Delta\theta}$ of 2.84×10^{-8} rad m^{-1}/V. The relationship of the intensity difference between two output beams and $\Delta\theta$ can be derived by the Jones matrix–formulation method as

$$\begin{bmatrix} E_1 \\ E_2 \end{bmatrix} = \begin{bmatrix} \cos(\pi/4) & \sin(\pi/4) \\ -\sin(\pi/4) & \cos(\pi/4) \end{bmatrix} \begin{bmatrix} \exp(j\Psi) & 0 \\ 0 & 1 \end{bmatrix} \times \begin{bmatrix} \cos\Delta\theta_R & \sin\Delta\theta_R \\ -\sin\Delta\theta_R & \cos\Delta\theta_R \end{bmatrix} \begin{bmatrix} \exp(j\Gamma_R) & 0 \\ 0 & 1 \end{bmatrix} \times \begin{bmatrix} \cos\Delta\theta_R & -\sin\Delta\theta_R \\ \sin\Delta\theta_R & \cos\Delta\theta_R \end{bmatrix} \begin{bmatrix} \cos\Delta\theta_I & \sin\Delta\theta_I \\ -\sin\Delta\theta_I & \cos\Delta\theta_I \end{bmatrix} \times \begin{bmatrix} \exp(j\Gamma_I) & 0 \\ 0 & 1 \end{bmatrix} \begin{bmatrix} \cos\Delta\theta_I & -\sin\Delta\theta_I \\ \sin\Delta\theta_I & \cos\Delta\theta_I \end{bmatrix} \begin{bmatrix} 1 \\ 0 \end{bmatrix} \sqrt{I_o}. \tag{7}$$

The first matrix in Eq. (7) is for the analyzer rotated by 45°, and the second is for the compensator rotated by 90° with respect to the x axis, as shown in Fig. 1. Ψ is the retardation value achieved by the compensator. The third to fifth and sixth to eighth matrices correspond to reflected and incident probe beams, respectively, propagating within the crystal. $\Delta\theta_I$ is the slight rotation angle of the principal axes for the incident beam propagating within the crystal as described by approximation (6), and Γ_I is the total phase retardation of the incident beam propagating within the crystal induced by changes in both the static-index difference and the EO-index difference. The static-index difference here is 4×10^{-3}, whereas the change in EO-index difference is less than 10^{-8} when $E_x = 10^4$ V/m, which is a typical E-field strength value when 10 V is applied to a metal gap with 1-mm spacing. Therefore, in this EO probing configuration, Γ_I is approximately equal to the value induced by the portion of static-index difference only, which is

$$\Gamma_I = 2\pi(n_e - n_o)(L/\lambda). \tag{8}$$

Similarly, $\Delta\theta_R$ and Γ_R are those values for the reflected probe beam that propagates within the crystal and can be obtained in the same way. Inasmuch as $\Delta\theta_I$ is small, the sixth to eighth matrices in Eq. (7) can be approximated as

$$\begin{aligned} &\begin{bmatrix} 1 & \Delta\theta_I \\ -\Delta\theta_I & 1 \end{bmatrix} \begin{bmatrix} \exp(j\Gamma_I) & 0 \\ 0 & 1 \end{bmatrix} \begin{bmatrix} 1 & -\Delta\theta_I \\ \Delta\theta_I & 1 \end{bmatrix} \\ &\quad = \begin{bmatrix} \exp(j\Gamma_I) + (\Delta\theta_I)^2 & [1 - \exp(j\Gamma_I)]\Delta\theta_I \\ [1 - \exp(j\Gamma_I)]\Delta\theta_I & 1 + \exp(j\Gamma_I)(\Delta\theta_I)^2 \end{bmatrix} \\ &\quad \approx \begin{bmatrix} \exp(j\Gamma_I) & [1 - \exp(j\Gamma_I)]\Delta\theta_I \\ [1 - \exp(j\Gamma_I)]\Delta\theta_I & 1 \end{bmatrix}. \end{aligned} \tag{9}$$

Similarly, an approximation for the third to fifth matrices can be obtained. Substituting the two approximation matrices into Eq. (7), we can rewrite that equation as

$$\begin{bmatrix} E_1 \\ E_2 \end{bmatrix} = \sqrt{\frac{I_o}{2}} \begin{bmatrix} \exp[j(\Gamma_I + \Gamma_R + \Psi)] - \exp[j(\Gamma_I + \Gamma_R)]\Delta\theta_R + \exp(j\Gamma_I)(\Delta\theta_R - \Delta\theta_I) + \Delta\theta_I \\ -\exp[j(\Gamma_I + \Gamma_R + \Psi)] - \exp[j(\Gamma_I + \Gamma_R)]\Delta\theta_R + \exp(j\Gamma_I)(\Delta\theta_R - \Delta\theta_I) + \Delta\theta_I \end{bmatrix}. \tag{10}$$

Then the intensity difference between the two output beams for the HR-type probe tip can be expressed as

$$\begin{aligned} \Delta I_{\theta,\mathrm{HR}} &= |E_1|^2 - |E_2|^2 \\ &= 2I_o\{[-\Delta\theta_R \cos(\Gamma_I + \Gamma_R) + (\Delta\theta_R - \Delta\theta_I) \\ &\quad \times \cos\Gamma_I + \Delta\theta_I]\cos(\Gamma_I + \Gamma_R + \Psi) \\ &\quad + [-\Delta\theta_R \sin(\Gamma_I + \Gamma_R) + (\Delta\theta_R - \Delta\theta_I)\sin\Gamma_I] \\ &\quad \times \sin(\Gamma_I + \Gamma_R + \Psi)\}. \end{aligned} \tag{11}$$

Because $\Gamma_I = \Gamma_R = \Gamma$ and $\Delta\theta_I = -\Delta\theta_R = \Delta\theta$, Eq. (11) can be rewritten as

$$\Delta I_{\Delta\theta,\mathrm{HR}} = 4I_o(\cos\Gamma - 1)\cos(\Gamma + \Psi)\Delta\theta. \tag{12}$$

For a given Γ value that corresponds to a fixed crystal length, $\Delta I_{\Delta\theta,\mathrm{HR}}$ has the extreme E_x response when retardation Ψ of the compensator is tuned to

$$\Psi = -\Gamma \pm m\pi \qquad (m \text{ an integer}) \tag{13}$$

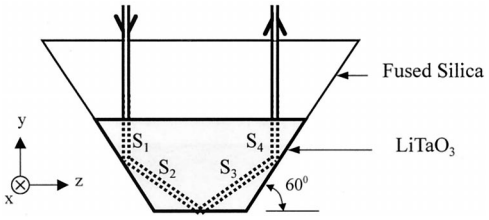

Fig. 2. Side view of a TIR probe tip and illustration of the four segments for the probe beam.

and the maximum response is

$$|\Delta I_{\Delta\theta,\mathrm{HR}}| = 4I_o(1 - \cos\Gamma)k_{\Delta\theta}E_x. \tag{14}$$

Therefore we can obtain E_x by measuring $\Delta I_{\Delta\theta,\mathrm{HR}}$ induced by the rotation of the new principal axes. It can be seen that the response vanishes if $\Gamma = 2n\pi$ and reaches its maximum when $\Gamma = (2n + 1)\pi$ (n an integer); i.e.,

$$|\Delta I_{\Delta\theta,\mathrm{HR}}| = \begin{cases} 0 & L = n\lambda/(n_e - n_o) \\ 4I_o k_{\Delta\theta}E_x & L = (n + 1/2)\lambda/(n_e - n_o) \end{cases}. \tag{15}$$

In a real situation, it does not seem easy to control the crystal tip such that it is exactly the length that will yield the maximum response; however, it is easy to avoid the vanishing response by polishing the crystal tip a bit to reduce its length if the crystal tip is the exact length that is necessary for the vanishing response.

The total internal reflection (TIR) probe tip described in Refs. 17 and 18 is another popular and important probe tip. It also can be used for the same measurements, and its performance may be superior to that of the HR type. The TIR geometry causes the optical beam to reflect from the bottom surface of the probe tip without requiring a HR coating. It is an ideal tip for external EO probing, and there are some advantages in this new modulation technique. The TIR probe tip and the arrangement of the beam propagation path are shown in Fig. 2. To proceed to its EO analysis, we decompose the path into four segments, S_1, S_2, S_3, and S_4; then the procedure described above for the HR probe tip can also be applied to each segment. If the HR probe tip in Fig. 1 is replaced by a TIR-type probe tip for a probe beam polarized at 45° with respect to the x axis to measure E_z, the intensity difference at the output becomes

$$\Delta I_{\Delta n,\mathrm{TIR}} = I_o \frac{2\pi}{\lambda}\left(\sum_{i=1}^{4} k_{\Delta n_i} 2L_i\right)E_z, \tag{16}$$

where L_i and $k_{\Delta n_i}$ are the length and the coefficient, respectively, of the change in the EO-index difference of ith segment S_i when E_z exists. $k_{\Delta n_1} = k_{\Delta n_4} = 1.14 \times 10^{-10}$ m/V and $k_{\Delta n_2} = k_{\Delta n_3} = 2.83 \times 10^{-11}$ m/V, whereas the corresponding coefficients of the change in the EO-index difference for E_x are $\sim 6 \times 10^{-14}$ m/V and can be neglected when they are compared with those for E_z.

For the same reasons as those for the HR-type tip, the response for this configuration is insensitive to E_x.

For the probe beam polarized along the x axis to measure E_x, the approximate result of the intensity difference for two output beams is

$$\begin{aligned}\Delta I_{\Delta\theta,\mathrm{TIR}} = 2I_o\Bigg\{\Bigg[&-\Delta\theta_4 \cos\left(\sum_{i=1}^{4}\Gamma_i\right) + (\Delta\theta_4 - \Delta\theta_3) \\ &\times \cos\left(\sum_{i=1}^{3}\Gamma_i\right) + (\Delta\theta_3 - \Delta\theta_2)\cos\left(\sum_{i=1}^{2}\Gamma_i\right) + (\Delta\theta_2 \\ &- \Delta\theta_1)\cos\Gamma_1 + \Delta\theta_1\Bigg]\cos\left(\sum_{i=1}^{4}\Gamma_i + \Psi\right) \\ &+ \Bigg[-\Delta\theta_4 \sin\left(\sum_{i=1}^{4}\Gamma_i\right) + (\Delta\theta_4 - \Delta\theta_3)\sin\left(\sum_{i=1}^{3}\Gamma_i\right) \\ &+ (\Delta\theta_3 - \Delta\theta_2)\sin\left(\sum_{i=1}^{2}\Gamma_i\right) + (\Delta\theta_2 \\ &- \Delta\theta_1)\sin\Gamma_1\Bigg]\sin\left(\sum_{i=1}^{4}\Gamma_i + \Psi\right)\Bigg\},\end{aligned} \tag{17}$$

where Γ_i and $\Delta\theta_i = k_{\Delta\theta_i}E_x$ correspond to the static phase retardation and the principal axis-rotation angle of the ith segment S_i. Γ_1 and $\Delta\theta_1$ are the same as Γ_I and $\Delta\theta_I$ and Γ_4 and $\Delta\theta_4$ are the same as Γ_R and $\Delta\theta_R$, respectively. Segments S_2 and S_3 correspond to the portions of the oblique incident path to the bottom surface and the reflection path of the optical beam, respectively. The method for finding the polarization vectors of normal modes and the corresponding refractive indices are described in many books (see, e.g., Refs. 16 and 19), and the calculated proportional constant $k_{\Delta\theta}$ for the EO rotation angle induced by E_x in approximation (6) is $k_{\Delta\theta_2} = -5.71 \times 10^{-8}$ rad m^{-1}/V for segment S_2 and $k_{\Delta\theta_3} = 5.54 \times 10^{-8}$ rad m^{-1}/V for segment S_3. Γ_2 and Γ_3 are again given by

$$\Gamma_i = 2\pi(n_e' - n_o)\frac{L_i}{\lambda}, \quad i = 2, 3. \tag{18}$$

The portion of the paths that is due to EO-induced index variation is neglected again, and $n_e' - n_o$ is equal to 9.979×10^{-4}. L_2 and L_3 are the lengths of segments S_2 and S_3, respectively. From Eq. (17) it can be expected that one can adjust more factors to avoid the vanishing response; for example, shifting the reflective spot position of the optical beam can change the length of each segment, which will result in a change of each Γ_i. For the same reason as that for the HR-type probe tip discussed above, the intensity difference of the TIR-type probe tip for this configuration is also insensitive to E_z.

The calculated E_x responses of the HR- and TIR-type probe tips are compared in Fig. 3; where the numerical and approximate results for two types of probe tip are also compared. The maximum E-field strength used in the calculations is 10^4 V/m. Figure 3 shows that the TIR-type probe tip has a better E_x response than the HR type.

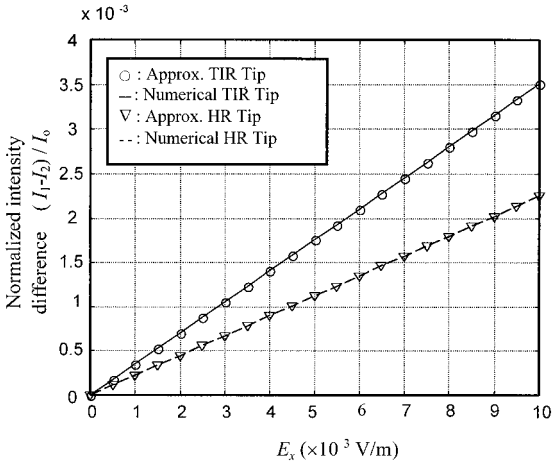

Fig. 3. Comparison of results of calculating E_x responses of the HR- and TIR-type probe tips.

3. Two-Dimensional E-Field Vector Measurement

For both the HR- and the TIR-type probe tips, only a single probe beam is needed for both E_x and E_z measurements, which one makes by switching the polarization orientations of the input probe beam to 90° and to 45° with respect to the x axis. Nevertheless, with this method, only E_x or E_z can be measured at one time. Measuring two components simultaneously requires two probe beams with the same propagation path but different input polarization orientations for a HR- or TIR-type probe tip. However, for the TIR probe tip there is an alternative method.

Consider a probe tip with the geometry shown in Fig. 4. It has four inclined planes, which can support two TIR beams with beam paths, one in the yz plane and the other in the xy plane, orthogonal to each other. Beam B_1 in the yz plane has the same propagation path as beam S_1 in Fig. 2, whereas beam B_2 has the path of beam S_2. To analyze the E_z response for beam B_2, we also decompose beam B_2 into four segments, as in Fig. 2. With the method described in Ref. 18 it can be calculated that all the segments of beam B_2 have the same E_z response, with a slope of -1.14×10^{-10} m/V for a change in index difference, whereas beam B_1 has two different responses for different segments. For beam B_1, both segments S_1 and S_4 have responses with a slope of 1.14×10^{-10} m/V for an EO change in the index difference, whereas both S_2 and S_3 have responses

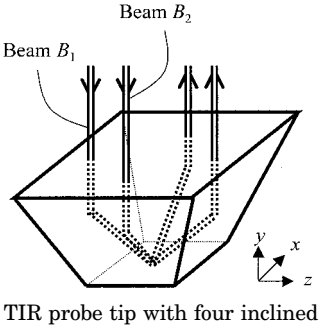

Fig. 4. TIR probe tip with four inclined planes.

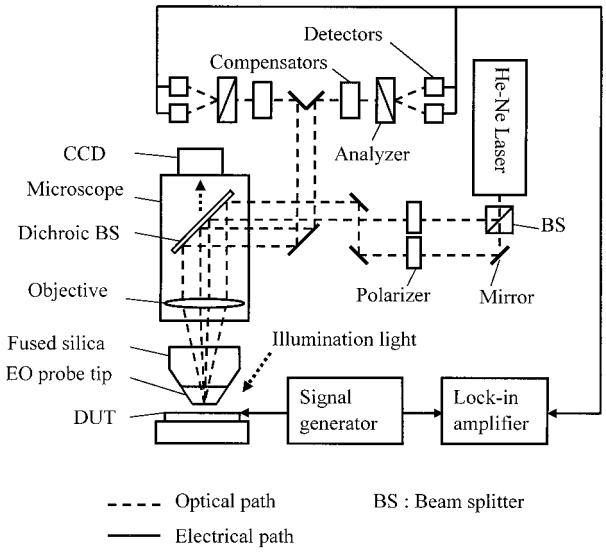

Fig. 5. Setup of the experimental system.

with a slope of 0.283×10^{-10} m/V, as described in Section 2. Because the dimensions of the bottom plane of the TIR tip are approximately 200 μm × 200 μm and the thickness of the tip is 120 μm, the angle between the inclined plane and the horizontal is 60°. The length of both segments S_1 and S_4 is 33 μm, and that of both segments S_2 and S_3 is $100\sqrt{3}$ μm. Therefore the ratio of E_z measurement sensitivity between beams B_2 and B_1 based on Eq. (16) can be estimated as

$$\frac{(100\sqrt{3} + 100\sqrt{3}) \times 1.14 + (33 + 33) \times 1.14}{(100\sqrt{3} + 100\sqrt{3}) \times 0.283 + (33 + 33) \times 1.14} = 2.71. \quad (19)$$

Obviously, this equation illustrates that the E_z response of beam B_2 is superior to that of beam B_1. Therefore, when this TIR tip with these two probe beams, B_1 and B_2, is used for the 2-D E-field vector measurement, for high sensitivity beam B_2 it is better to assign for the E_z measurement. The same calculation shows that beam B_1 has E_x response that is superior to that of beam B_2. Therefore, it is better to assign beam B_1 for the E_x measurement.

4. System Setup

The experimental setup for measurement of two tangential E-field components is shown in Fig. 5. A commercial microscope was adapted to this experimental system. A continuous-wave He–Ne laser with a wavelength of 632.8 nm and power of 5 mW was used as the probe beam. The $LiTaO_3$ TIR EO probe tip was supported by fused silica for convenience in mounting it upon a cantilevered beam. The four inclined planes of the EO probe tip were polished to prevent scattering loss. The optical beam from the He–Ne laser was split into two beams of equal intensity by a beam splitter, and one beam was bent three times such that the beams were parallel. The two beams passed individually through a

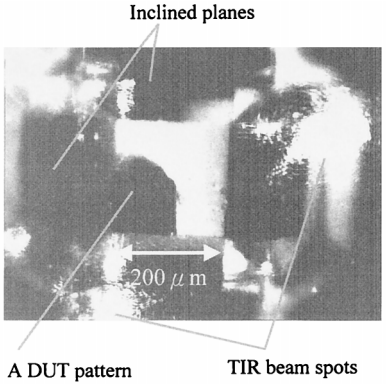

Fig. 6. CCD image of two TIR beam spots and the DUT pattern.

polarizer such that they had different linear polarizations. If the system is used for 2-D E-field measurement, one polarizer is rotated 45° with respect to the x axis of the EO crystal and the other polarizer lies on the x axis.

A dichroic beam splitter directs light to a CCD camera for optical observation. The light reflected from the DUT could also pass through the bottom surface of the TIR tip, which has no HR coating. This kind of EO probe tip allows us to observe where the TIR beam spot and the DUT pattern are. The observed CCD image is shown in Fig. 6. This makes it possible to know which point on the DUT is being measured.

After TIR from the probe tip, these two beams were fed into two individual compensators and analyzers and finally received by detectors. The differential signal between two detectors was measured with a lock-in amplifier. The test E field was generated by a signal generator that can produce a square waveform as the chopped static E field in the DUT. The synchronized signal of this waveform was used as the reference input for the lock-in amplifier. For this signal detection method, only the signals at the fundamental of the square waveform were amplified, and the detection bandwidth was 1 or 10 Hz. Therefore, noise was suppressed and sensitivity was greatly improved.

5. Experiments and Measurement Results

In the experiments we made some measurements with the system setup proposed in Section 4 to verify the discussions in Sections 2 and 3, and thus a 2-D E-field vector measurement was effectively accomplished.

In the first experiment we verified that our system with the beam propagation shown in Fig. 4 demonstrates higher sensitivity for E_z with beam B_2 propagating in the xy plane than with beam B_1 propagating in the yz plane, and the sensitivity ratio was as given in Eq. (19). In this experiment, a coplanar strip transmission line (CPSTL) with a spacing of 1 mm between two metal lines upon a dielectric substrate was used as the test pattern, which produced a uniform parallel E-field across the air between two metal lines when voltage was applied. If the probe tip was placed at a position centered between these two metal lines, the vertical E_y component could be small and negligible, as illustrated in the schematic diagram in Fig. 7. Figure 7(a) is the side view and Fig. 7(b) is the front view; the principal axes for each are also indicated. The CPSTL pattern can be used to generate an E field in the z-axis direction only. As both beam B_1 propagating in the yz plane and beam B_2 propagating in the xy plane are used to sense the E_z component, we rotated two polarizers 45° with respect to the x axis to detect the intensity difference that is due to the EO-index change. Two compensators were tuned to place each probe beam on a quarter-wave bias point such that the intensity difference was proportional to the EO-index change, as discussed above. The recorded lock-in amplifier readings are illustrated in Fig. 8, which shows that the E_z response of beam B_2 is better than that of beam B_1 by a factor of 2.85, which is quite

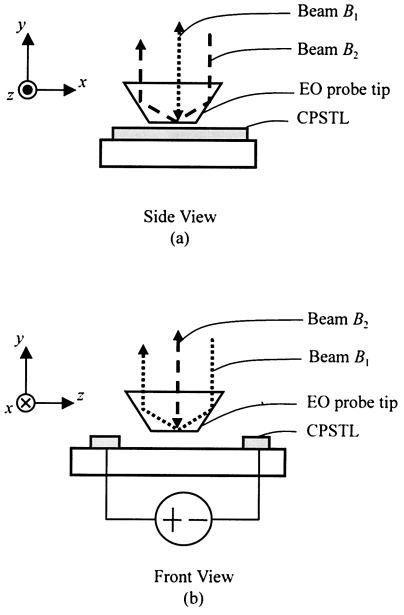

Fig. 7. Arrangement of the CPSTL and the EO probe tip for comparison of the E_z responses for beams B_1 and B_2.

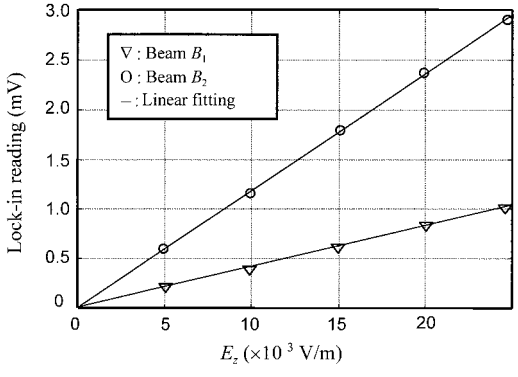

Fig. 8. Comparison of experimental results of the E_z responses for beams B_1 and B_2.

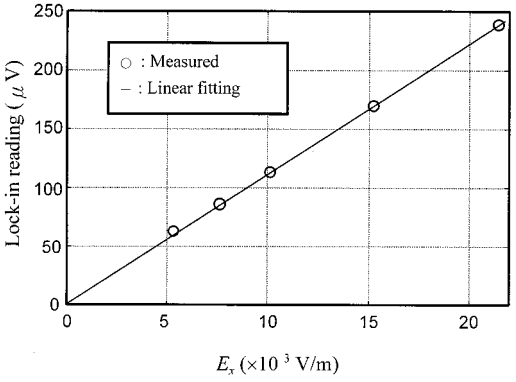

Fig. 9. Experimental result of the E_x response for beam B_1.

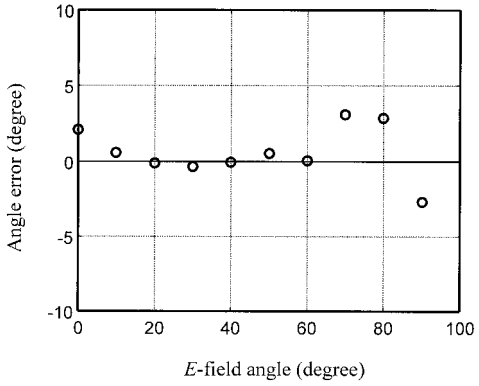

Fig. 10. Angle error in measurement of the E-field direction.

consistent with the value of 2.71 obtained from Eq. (19). In this E_z sensing experiment, sensitivities as great as 76 mV/cm/$\sqrt{\text{Hz}}$ for beam B_2 and 217 mV/cm/$\sqrt{\text{Hz}}$ for beam B_1 were achieved.

In the second experiment we measured the E_x component with beam B_1 polarized in the x direction; i.e., the polarizer was rotated along the direction of the x axis. A rotation stage underneath the CPSTL device as shown in Fig. 7 was rotated by 90° to generate the E_x component. For this case the recorded lock-in amplifier readings are shown in Fig. 9. In this E_x sensing experiment a sensitivity of 0.8 V/cm/$\sqrt{\text{Hz}}$ for beam B_1 was achieved. In addition, to confirm that this x-polarized beam in this configuration is insensitive to the E_z component, as discussed in Section 2, we rotated the CPSTL device 90° back to its original direction to generate the E_z component only. We found that the sensed reading was less than a tenth of that when the E_x component was applied, as expected.

The main goal with our measurement system is to sense 2-D E-field vectors. Before performing this measurement, we demonstrate the method for measurement of the 2-D E-field direction for a simple structure first. In this experiment, we used beam B_2 propagating in the xy plane to measure the E_z component and beam B_1 propagating in the yz plane to measure the E_x component, as discussed above. The CPSTL pattern shown in Fig. 7 was used again. The CPSTL was rotated to form an angle between the c axis (i.e., the z axis) of the EO crystal, and the direction of the E field from 0° to 90° in increments of 10°. The angle error, in degrees, between the measured E field and the E field setup by the rotation stage is shown in Fig. 10. A root-mean-square error of 1.5° was achieved, which shows the suitability of our system for the direction measurment of an E-field vector.

Finally, we used the system to sense 2-D E-field vectors on a test pattern. In this experiment we again used beam B_2 propagating in the xy plane and beam B_1 propagating in the yz plane were used again to measure the E_z and E_x components, respectively. The test pattern comprised two rectangular metal plates upon a dielectric substrate with widths of 2 mm and spaced 0.5 mm apart, as shown in Fig. 11. A voltage was applied between these two metal plates, as shown in the figure. The EO probe tip was placed 20 μm above the metal pattern. The 2-D E-field vectors, which contained both E_x and E_z components, were measured along the trajectory of the dashed line in the middle of the gap, as indicated. For this test path, vertical E_y components were small and sensitivities of both of the probe beams for the E_y component were much lower than those for the E_x and E_z components; therefore the E_y effects could be neglected. The distance between two measured points was 0.1 mm. Measured results and the simulation results obtained with an Ansoft Maxwell three-dimensional field simulator, which are in good agreement, are shown in Fig. 12. The experimental results show the feasibility of using our system to sense 2-D E-field vectors.

6. Conclusions

Measurement of a 2-D E-field vector by a $LiTaO_3$ EO probe tip has been demonstrated. We used a conventional EO modulation technique based on the change in index difference and a new one based on rotation of the principal axis to resolve two E-field components simultaneously. A theory of this new modulation technique was derived, and experiments were performed to verify its validity. The results for 2-D E-field vector measurement were in good agreement with the simulation by a commercial three-dimensional E-field simulator. The sensitivities for two tangential E-field components were 76 (mV/cm)/$\sqrt{\text{Hz}}$ and 0.8 (V/cm)/$\sqrt{\text{Hz}}$ for E_x and E_z, respec-

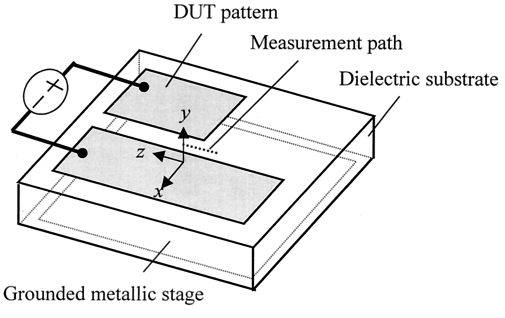

Fig. 11. Test pattern for measurement of the 2-D E-field vector.

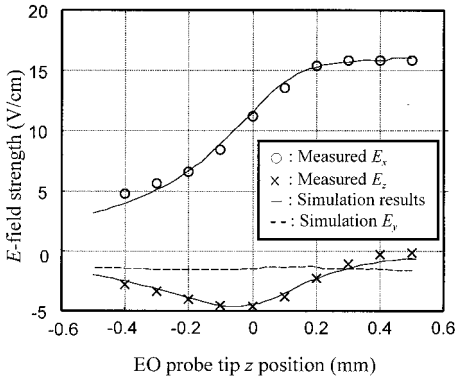

Fig. 12. Results of measurement of the 2-D E-field vector.

tively, and the root-mean-square error of the E-field direction measurement was 1.5°. This study extends the EO sensing technique to measure the vector E-field signal, which cannot be obtained with a traditional electric probe tip. If the probe source is replaced by a pulsed laser, one can use this technique to analyze microwave circuits and the near-field radiation pattern of planar antennas. It will be an effective tool for the design and testing of microwave devices and circuits.

Appendix A

Consider an input beam polarized at 45° with respect to the x axis propagating into a $LiTaO_3$ EO crystal along the y axis with E_x included.

The Jones matrix formulation for this system is

$$\begin{bmatrix} E_1 \\ E_2 \end{bmatrix} = \begin{bmatrix} \cos(\pi/4) & \sin(\pi/4) \\ -\sin(\pi/4) & \cos(\pi/4) \end{bmatrix} \begin{bmatrix} \exp(j\varphi) & 0 \\ 0 & 1 \end{bmatrix} \begin{bmatrix} \cos(-\alpha) & \sin(-\alpha) \\ -\sin(-\alpha) & \cos(-\alpha) \end{bmatrix} \begin{bmatrix} \exp(j\delta) & 0 \\ 0 & 1 \end{bmatrix} \begin{bmatrix} \cos(-\alpha) & -\sin(-\alpha) \\ \sin(-\alpha) & \cos(-\alpha) \end{bmatrix} \times \begin{bmatrix} \cos\alpha & \sin\alpha \\ -\sin\alpha & \cos\alpha \end{bmatrix} \begin{bmatrix} \exp(j\delta) & 0 \\ 0 & 1 \end{bmatrix} \begin{bmatrix} \cos\alpha & -\sin\alpha \\ \sin\alpha & \cos\alpha \end{bmatrix} \begin{bmatrix} 1/\sqrt{2} \\ 1/\sqrt{2} \end{bmatrix} \sqrt{I_o}$$
$$\approx \frac{\sqrt{I_o}}{2} \begin{bmatrix} \exp j(2\delta + \varphi) + \alpha[1 - \exp(j\delta)]^2[1 - \exp(j\varphi)] + 1 \\ -\exp j(2\delta + \varphi) + \alpha[1 - \exp(j\delta)]^2[1 + \exp(j\varphi)] + 1 \end{bmatrix}$$
$$= \frac{\sqrt{I_o}}{2} \begin{bmatrix} A + B + i(C + D) \\ A - B + i(C - D) \end{bmatrix}, \tag{A1}$$

where

$$A = \alpha(1 - 2\cos\delta + \cos 2\delta) + 1,$$
$$B = \cos(2\delta + \varphi) - \alpha[\cos\varphi - 2\cos(\delta + \varphi) + \cos(2\delta + \varphi)],$$
$$C = \alpha(-2\sin\delta + \sin 2\delta),$$
$$D = \sin(2\delta + \varphi) - \alpha[\sin\varphi - 2\sin(\delta + \varphi) + \sin(2\delta + \varphi)],$$

φ is the retardation of the compensator, α is the slight rotation angle of the principal axes induced by E_x for the incident beams propagating within the $LiTaO_3$ EO crystal, and δ is the total retardation, which includes both a static portion and an EO-induced portion. As α is small, a discussion similar to that for Eq. (7) in Section 2 and the same approximation technique as for Eq. (9) are used, and the high-order terms are neglected. The intensity difference at the output is then given as

$$\begin{aligned} \Delta I &= |E_1|^2 - |E_2|^2 \\ &= \frac{I_o}{4}\{[(A + B)^2 + (C + D)^2] - [(A - B)^2 + (C - D)^2]\} \\ &= I_o(AB + CD) \\ &\approx I_o\{\alpha(1 - 2\cos\delta + \cos 2\delta)\cos(2\delta + \varphi) - \alpha[\cos\varphi - 2\cos(\delta + \varphi) + \cos(2\delta + \varphi)] + \cos(2\delta + \varphi) + \alpha(-2\sin\delta + \sin 2\delta)\sin(2\delta + \varphi)\} \\ &= I_o\cos(2\delta + \varphi), \end{aligned} \tag{A2}$$

where the high-order terms are neglected. It is obvious that the intensity is independent of the slight rotation value α. Therefore the intensity difference is insensitive to E_x.

The authors thank the National Center for High-Performance Computing National Science Council, Republic of China, for its support in our use of simulation hardware and software.

References

1. J. A. Valdmanis, G. Mourou, and C. W. Gaabel, "Picosecond electro-optic sampling system," Appl. Phys. Lett. **41,** 211–212 (1982).
2. K. W. Chang and W. V. Sorin, "Electro-optic sampling of high speed nonlinear device," in *Ultrafast Electronics and Optoelectronics*, J. Shah and U. Mishra, eds., Vol. 14 of OSA Procedings Series (Optical Society of America, Washington, D.C., 1993), pp. 220–223.
3. J. A. Valdmanis and S. S. Pei, "A non-contact picosecond prober for intergrated circuit testing," in *Picosecond Electronics andOptoelectronics*, F. J. Leonberger, C. H. Lee, F. Capasso, and H. Morkoc, eds. (Springer-Verlag, New York, 1987).
4. S. L. Huang, C. H. Lee, and H.-L. A. Huang, "Real-time linear

time-domain network analysis using picosecond photoconductive mixer and samplers," IEEE Trans. Microwave Theory Tech. **43,** 1281–1289 (1995).
5. M. G. Li, E. V. Chauchard, C. H. Lee, and H.-L. A. Hung, "Two-dimension field mapping of GaAs microstrip circuit by electro-optic sensing," in *Picosecond Electronics and Optoelectrics*, F. J. Leonberger, C. H. Lee, F. Capasso, and H. Morkoc, eds. (Springer-Verlag, New York, 1987), pp. 54–58.
6. B. H. Kolner and D. M. Bloom, "Electrooptic sampling in GaAs integrated circuits," IEEE J. Quantum Electron. **QE-22,** 79–93 (1986).
7. M. S. Heutmaker and G. T. Harvey, "Electro-optic sampling of high-speed silicon integrated circuits using a GaAs probe tip," Appl. Phys. Lett. **59,** 146–148 (1991).
8. D. L. Quang, D. Erasme, and B. Huyart, "Fabry–Perot enhanced real-time electro-optic probing of MMICs," Electron. Lett. **29,** 498–499 (1993).
9. H. Takahashi, S.-I. Aoshima, and Y. Tsuchiya, "Sampling and real-time methods in electro-optic probing system," IEEE Trans. Instrum. Meas. **44,** 965–971 (1995).
10. T. K. Ishii, *Microwave Engineering*, 2nd ed. (Harcourt Brace Jovanovich, San Diego, Calif., 1989).
11. T. Pfeifer, T. Loffler, H. G. Roskos, H. Kurz, M. Singer, and E. M. Biebl, "Electro-optic near-field mapping of planar resonators," IEEE Trans. Antennas Propag. **46,** 284–291 (1998).
12. K. Kamogawa, I. Toyoda, K. Nishikawa, and T. Tokumitsu, "Characterization of a monolithic slot antenna using an electro-optic sampling technique," IEEE Microwave Guided Wave Lett. **4,** 414–416 (1994).
13. Y. Imaizumi, M. Shinagawa, and H. Ogawa, "Electric field distribution measurement of microstrip antenna and arrays using electro-optic sampling," IEEE Trans. Microwave Theory Tech. **43,** 2402–2047 (1995).
14. W. K. Kuo, S. L. Huang, and L. C. Chang, "On-wafer dual-beam electro-optic probing of electric-field vector," in Digest of Conference on Lasers and Electro-Optics, Vol. 11 of 1997 OSA Technical Digest Series (Optical Society of America, Washington, D.C., 1997). 142–143 (1997).
15. W. K. Kuo, S. L. Huang, T. S. Horng, and L. C. Chang, "Two-dimensional mapping of electric-field vector by electro-optic prober," Opt. Commun. **149,** 55–60 (1998).
16. A. Yariv and P. Yeh, *Optical Waves in Crystal* (Wiley, New York, 1984).
17. M. Y. Frankel, S. Gupta, J. A. Valdmanis, and G. A. Mourou, "Terahertz attenuation and disperation characteristics of coplanar transmission lines," IEEE Trans. Microwave Theory Tech. **39,** 910–916 (1991).
18. J. Nees and G. A. Mourou, "Noncontact electro-optic sampling with a GaAs injection laser," Electron. Lett. **22,** 918–919 (1986).
19. W. M. Robertson, *Optoelectronic Techniques for Microwave and Millimeter-Wave Engineering* (Artech House, Boston, Mass., 1995).